

ANGULAR DEPENDENCE OF RAMAN SCATTERING SELECTION RULES FOR LONG-WAVELENGTH OPTICAL PHONONS IN SHORT-PERIOD GaAs/AlAs SUPERLATTICES

V. A. Volodin^{a,b*}, V. A. Sachkov^c, M. P. Sinyukov^a

^a Rzhanov Institute of Semiconductor Physics, Siberian Division, Russian Academy of Sciences
630090, Novosibirsk, Russia

^b Novosibirsk State University
630090, Novosibirsk, Russia

^c Omsk Scientific Center, Siberian Branch, Russian Academy of Sciences
644024, Omsk, Russia

Received February 16, 2016

The angular dependence of Raman scattering selection rules for optical phonons in short-period (001) GaAs/AlAs superlattices is calculated and studied experimentally. Experiments are performed using a micro-Raman setup, in the scattering geometry with the wave vectors of the incident and scattered light lying in the plane of superlattices (so-called in-plane geometry). Phonon frequencies are calculated using the Born model taking the Coulomb interaction into account in the rigid-ion approximation. Raman scattering spectra are calculated in the framework of the deformation potential and electro-optical mechanisms. Calculations show an angular dependence of the selection rules for optical phonons with different directions of the wave vectors. Drastic differences in the selection rules are found for experimental and calculated spectra. Presumably, these differences are due to the Fröhlich mechanism in Raman scattering for short-period superlattices.

DOI: 10.7868/S004445101607018X

1. INTRODUCTION

Heterostructures with an artificial period are known as superlattices (SLs); their electronic, optical, and phonon properties depend on the period [1, 2]. The bright effects for phonons in SLs are a “folding” of acoustic phonon modes and localization of optical modes, which were observed by Raman light scattering [3–9]. With the advent of a micro-Raman technique, the possibilities of studying the angular dependence of optical phonons in SLs have appeared [10–18]. Typically, however, experimental works do not contain calculated data and theoretical works with a calculated phonon dispersion do not contain experimental data [19–21]. Thus, there is a lack of works in which the angular dependence of selection rules for Raman scattering in SLs is discussed [11, 13]. It is worth noting that only dispersion of phonons was calculated in [10–14], and no calculations of Raman spectra for different ge-

ometries were done. According to our knowledge, the contribution of the electro-optical mechanism to Raman scattering was poorly discussed. This work is an attempt to study the angular dependence of Raman scattering selection rules for long-wavelength optical phonons in short-period GaAs/AlAs SLs both experimentally and theoretically.

2. MATERIALS AND METHODS

The GaAs/AlAs SLs were grown using molecular beam epitaxy on a (001) GaAs substrate. First, thick GaAs and AlAs buffer layers were grown, and then alternating AlAs and GaAs layers consisting of 5, 7, or 9 monolayers (MLs) were produced. The parameters of superlattices are presented in Table 1. Some SLs were covered with a relatively thick protective GaAs layer because thin GaAs layers kept in air can be oxidized, while AlAs layers are chemically unstable, and therefore the whole SL can be oxidized. The Raman spectrometer T64000 (Horiba Jobin Yvon) with a micro-Raman setup based on an Olympus optical microscope

* E-mail: volodin@isp.nsc.ru

with a $\times 100$ high-aperture microscope lens (with the aperture-to-focus-length ratio 1/2.5) and the 514.5 nm line of an Ar⁺ laser were used. The spectral resolution was better than 2 cm⁻¹. The radiation power reaching the sample was ~ 1 mW, which is insufficient to cause significant heating of the sample. The spatial resolution is determined by the size of the laser beam at the focus and was equal to 1 micron. This allowed us to use the scattering geometry in which the wave vectors of the incident and scattered light lie in the plane of the SLs (in-plane geometry, as it was called in [11,13]). In these experiments, the light was focused onto specially made cleavages of SLs. This approach is described in more detail in [16,17].

3. RESULTS AND DISCUSSION

Figures 1–3 show the experimental (upper cases) and calculated (down cases) spectra of the SLs for the scattering geometries $X(ZY)-X$ and $X(YY)-X$. Here,

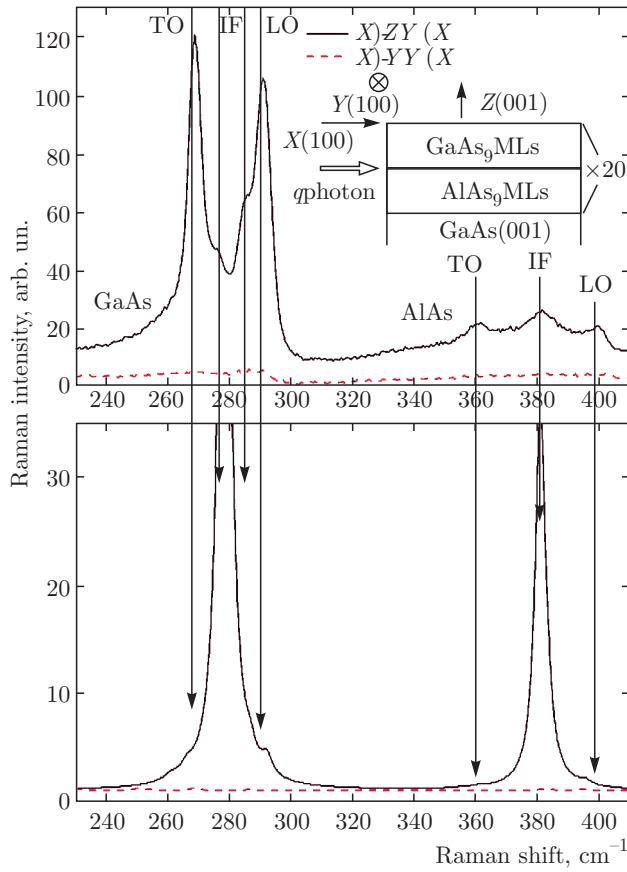


Fig. 1. Experimental (upper case) and calculated (lower case) Raman spectra of the GaAs₉/AlAs₉ superlattice. Inset: scheme of Raman scattering geometry

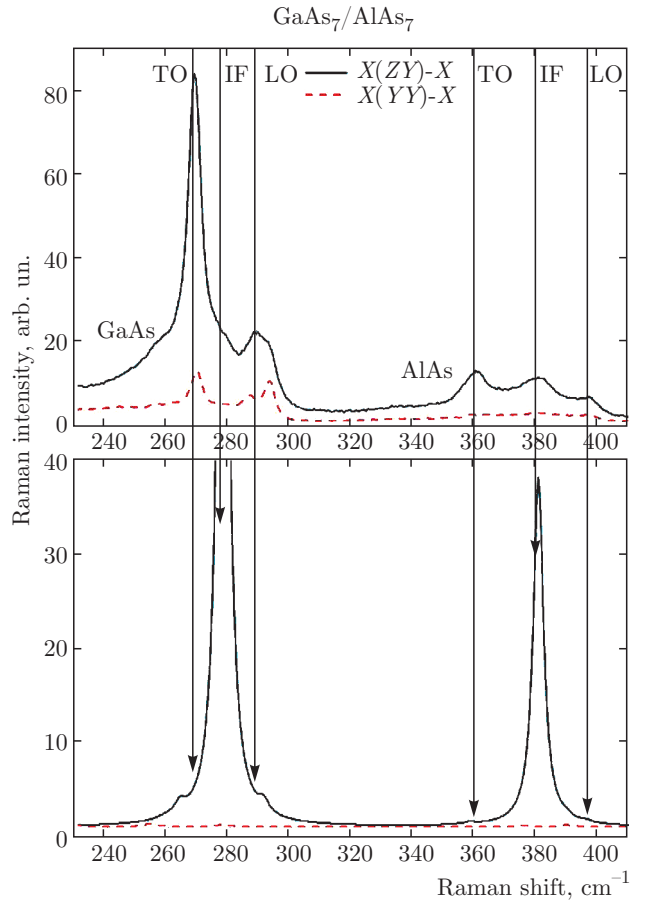


Fig. 2. Experimental (upper case) and calculated (lower case) Raman spectra of the GaAs₇/AlAs₇ superlattice

the axes in brackets correspond to directions of the polarization of the electric field vector of the incident and scattered electromagnetic waves, and the axes outside the brackets indicate the direction of the wave vector of the incident and scattered light (this is so-called Porto's notation). The axes X , Y , and Z correspond to crystallographic directions (100), (010), and (001). The Raman scattering tensors $D_{\alpha\beta}$ for phonons in bulk GaAs or AlAs with a wave vector along the Z axis and with different directions of atomic displacements (X , Y , or Z) are

$$\begin{aligned} \text{TO}_X & \left(\begin{array}{ccc} 0 & 0 & 0 \\ 0 & 0 & d \\ 0 & d & 0 \end{array} \right); \quad \text{TO}_Y \left(\begin{array}{ccc} 0 & 0 & d \\ 0 & 0 & 0 \\ d & 0 & 0 \end{array} \right); \\ \text{LO}_Z & \left(\begin{array}{ccc} 0 & d & 0 \\ d & 0 & 0 \\ 0 & 0 & 0 \end{array} \right), \end{aligned} \quad (1)$$

Table 1. Parameters of the SLs

№	GaAs, MLs	AlAs, MLs	Number of periods	Thickness, nm	Thickness of cap GaAs layer, nm
1	9	9	20	100	no cap
2	7	7	103	412	no cap
3	5	5	132	370	24

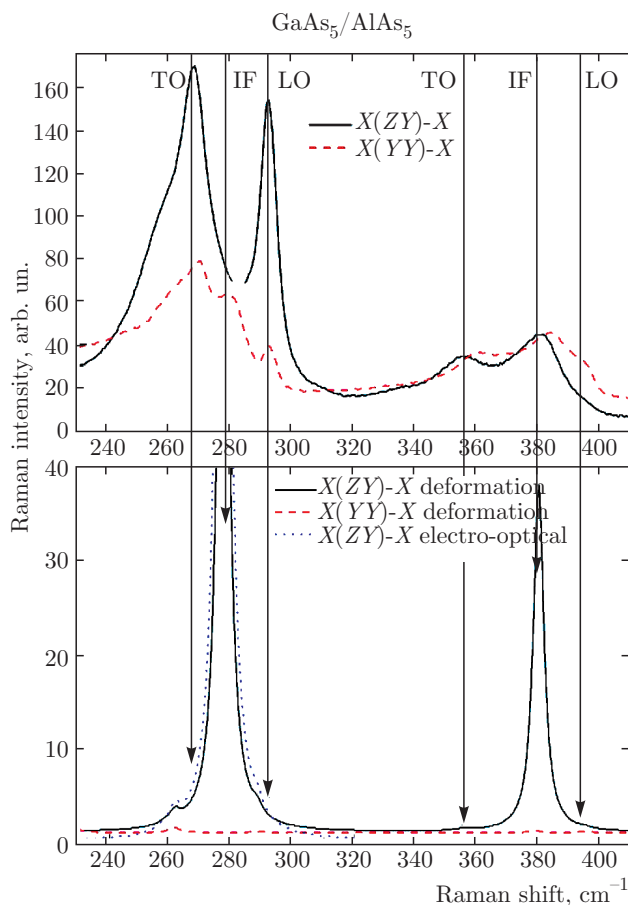


Fig. 3. Experimental (upper case) and calculated (lower case) Raman spectra of the $\text{GaAs}_5/\text{AlAs}_5$ superlattice. Dotted curve: the spectrum calculated using the electro-optic mechanism

where d is the additive differential polarizability of bonds. According to symmetry selection rules, the Raman intensity is proportional to $(E_{S,\alpha}D_{\alpha\beta}E_{i,\beta})^2$, where E_i is the polarization vector of the incident light and E_s is the polarization vector of the scattered light. Thus, for bulk GaAs or AlAs, only the $X(ZY)$ - X geometry is allowed for longitudinal optical (LO) phonons. The transverse optical (TO) phonons are forbidden for both geometries.

The phonon frequencies and Raman spectra were calculated using a phenomenological Born model (the two-particle interaction approximation) taking the interaction of an atom not only with nearest neighbors but also with atoms in the next coordination spheres into account (the so-called extended Born model). Phonons in GaAs/AlAs heterostructures were simulated by the mass-substitution method [22] based on the model parameters of gallium arsenide (in the case of an aluminum atom, only the mass was changed). The long-range Coulomb interaction was considered in the dipole approximation. The effective charge of cations and anions for GaAs was found from the difference of the squares of the longitudinal ($\omega_L = 292.6 \text{ cm}^{-1}$) and transverse ($\omega_T = 269 \text{ cm}^{-1}$) frequencies. The Raman line intensity for each mode was calculated in the Volkenshtein additive bond polarizability approximation [23]. This method is based on the assumption that each covalent bond has its own polarizability depending only on the bond length. Then the polarizability of the system can be represented as the sum of polarizabilities of all bonds [24]. The GaAs/AlAs heterostructure was calculated using parameters taken from [24]. The details of calculations are described elsewhere [17, 25]. For visual clarity, the peaks with low intensities and the vertical axes for all of the calculated spectra were omitted. The intensities of biggest GaAs-type IF-like modes were about 80 units in all cases (Figs. 1–3, lower plots). We have also calculated Raman spectra taking the electro-optical mechanism for both macroscopic and local electrical fields into account [26].

As we can see by comparing the experimental and calculated data, the main difference between them is the presence in the experimental spectra of the forbidden TO-like ($\sim 268 \text{ cm}^{-1}$) and LO-like ($\sim 290 \text{ cm}^{-1}$) modes for GaAs layers and also TO-like ($\sim 360 \text{ cm}^{-1}$) and LO-like ($\sim 400 \text{ cm}^{-1}$) modes for AlAs layers. For all spectra (Figs. 1–3), these modes are marked by arrows. As we can see, these modes have largest intensities in the experimental spectra, but are small and also somewhat shifted in the calculated ones.

It is known [11,13] that for flat SLs in the $X(ZY)$ - X geometry, only interface-like (IF-like) modes with frequencies depending on the GaAs/AlAs thickness ratio are allowed. For the SLs with similar GaAs and AlAs layer thicknesses, these frequencies are about the mean value between TO and LO phonon frequencies, $\sim 280 \text{ cm}^{-1}$ for phonons localized in GaAs layers and $\sim 380 \text{ cm}^{-1}$ for phonons localized in AlAs layers. These modes are also marked by arrows in Figs. 1–3. We can see that IF-like modes are present in the experimental spectra, but they are relatively small. For all SLs, the experimentally observed and calculated frequencies of IF-like modes for AlAs layers show good coincidence. For the GaAs₇/AlAs₇ and GaAs₅/AlAs₅ SLs (Figs. 2 and 3), the experimentally observed and calculated frequencies of IF-like modes for GaAs layers are also in good agreement. But the intensities of these modes are so small that they can be detected only after resolving the spectra into individual peaks. For the GaAs₉/AlAs₉ SL (Fig. 1), we can see two separate IF-like modes in experimental spectrum, but only one mode dominates in the calculated spectrum, weak features being barely distinguishable on its background. For readability, all calculated spectra in Figs. 1–3 are shown with breaks at the vertical axes. As regards the “forbidden” $X(YY)$ - X geometry, both experimental and calculated spectra have only very weak features, except GaAs₅/AlAs₅ SL (Fig. 3, experimental spectrum). We discuss this below.

It is worth noting that the spectra shown in Figs. 1–3 (lower plots) were calculated using only the deformation potential mechanism. We have also performed calculations of Raman spectra taking the electro-optical mechanism into account. It is known that the polarizability of a bond is the tensor

$$\begin{bmatrix} \alpha_{\parallel} & 0 & 0 \\ 0 & \alpha_{\perp} & 0 \\ 0 & 0 & \alpha_{\perp} \end{bmatrix}. \quad (2)$$

In the first-order approximation for a polar crystal, the polarizability of bonds depends on the parallel component of the electric field E_{\parallel} , and the additional polarizability is

$$\delta\alpha_{ij} = \begin{bmatrix} \frac{\partial\alpha_{\parallel}}{\partial E_{\parallel}} & 0 & 0 \\ 0 & \frac{\partial\alpha_{\perp}}{\partial E_{\parallel}} & 0 \\ 0 & 0 & \frac{\partial\alpha_{\perp}}{\partial E_{\parallel}} \end{bmatrix} \cos(\omega t) \cdot (\mathbf{E}_0 \mathbf{l}_k). \quad (3)$$

Here, the external electric field (which appears due to phonons in polar crystals) has the amplitude E_0 and alternates with the phonon frequency ω . The vector \mathbf{l}_k is directed along the k th bond in a unit cell. For a macroscopic electrical field (which is almost constant within a unit cell in the case of long-wavelength LO phonons), total effect from all bonds for Raman tensors in a crystal with the zinc blend structure is the same as in the case of the deformation potential mechanism (see tensors in formula (1)) for the X , Y , and Z components of the electric field. For the local electric field, we must calculate the electric field from the phonon in the middle of all bonds, and then we must add the effects from all bonds. For clarity, it is necessary to mention that in our case, a “local” electric field means the additional field caused by displacement of cations and anions due to a phonon mode. The field is different for different phonon modes. The procedure of calculating the Raman spectra using this approach was applied, but it turned out that the spectra calculated using the electro-optical mechanism for local electric fields are very similar to the spectra calculated using only the deformation potential mechanism. But, for a comparative analysis, this spectrum for GaAs₅/AlAs₅ SL is shown in Fig. 3 with the spectra calculated using only the deformation potential mechanism. We can see only weak differences for some low-intensity modes. We also see that the weak peaks in the calculated and experimental spectra have somewhat different frequencies. The modes with frequencies 267 and 291 cm^{-1} are not active with both the deformation potential and electro-optical mechanisms, and the question why they active in the experimental spectrum is discussed below.

The influence of the GaAs/AlAs interface disorder on Raman spectra was also calculated (similarly to the approach discussed in [17]). It was found that even total disordering and notflat (corrugated) interfaces do not lead to the appearance of intensive modes with frequencies 268 and 290 cm^{-1} in the calculated spectra (these modes can be seen in the experimental spectra). Hence, disordering cannot be the reason of the drastic breaking of the selection rules. The estimates of how “polarization leakage” due to the used high-aperture microscope lens can break the selection rules were done. Because the refractive index of the SL is high (about 4), the ratio of the parallel component of the wave number to the perpendicular component for quasi-backscattering in our case is about 1/10. Because the intensity of light is proportional to the square of the amplitude, the contribution of the effect of polarization leakage is small (about 1%).

Table 2. Components of the electrical momentum for calculated GaAs-like optical phonons in the $\text{GaAs}_5/\text{AlAs}_5$ superlattice

Frequency, cm^{-1}	Real part			Imaginary part		
	X	Y	Z	X	Y	Z
246.46	0.002	0.004	0.391	0	0.012	-0.074
258.06	0.078	0.002	-0.002	-0.061	-0.056	0
258.09	0.003	0.253	0.004	-0.057	-0.055	0.028
259.55	0.006	0	0	-0.003	-0.003	0
259.65	0	0	-0.003	0	0	-0.028
261.00	-0.138	0	0	0.010	0.013	0
261.08	0	-0.807	0	0.013	-0.017	0.016
261.47	-0.170	0	0	0	0.006	0
264.48	0	0	0	0	0	0
264.5	0	0.002	0.009	0	0	-0.203
267.84*	0	4.136	0	-0.005	0.165	0.030
273.36*	0	0.001	3.72	0	-0.002	0.123
277.07*	3.009	0	0	0.118	-0.009	0
282.17*	0	-0.001	3.728	0	0.051	0.165
288.13	0.003	0	0	-0.378	0	0

We note that, for example, the $\text{GaAs}_5/\text{AlAs}_5$ SL has 20 atoms in its unit cell. Hence, it has 60 phonon modes, 30 of which are optical modes. Fifteen modes of the 30 optical modes are GaAs-localized modes, but not all of them are Raman active. We have calculated frequencies, atomic displacements, and electrical dipole moments for all these 15 modes for the wave vector 10^6 cm^{-1} along the X axis. The results are shown in Table 2. We see that the mode that is Raman active in experiment, with the frequency about 268 cm^{-1} , has the largest dipole momentum. In Table 2, the modes with a large momentum are marked with an asterisk, and also with the boldface font. Analysis of the experimental spectra in Fig. 3 shows that in addition to the most intense peaks at the frequencies 267 and 291 cm^{-1} , there are also weaker peaks at 277 and 286 cm^{-1} . These frequencies are close to the frequencies of modes with large dipole momenta (see Table 2). Therefore, it is reasonable to assume that they can interfere with charged particles (electrons or holes) in SLs

due to Coulomb interaction. The Coulomb mechanism of electron–phonon interaction is known as the Fröhlich mechanism, taking place in transport phenomena and also in Raman scattering [2, 27–30]. It seems that the intensity of Fröhlich scattering can be proportional to the squared modulus of the dipole moments; such a “semiclassical” interpretation of the Fröhlich mechanism requires further investigations. The selection rules for the Fröhlich mechanism are different from the selection rules for the deformation potential mechanism [2, 13]. Our experimental spectra are similar to the spectra observed by Cardona with co-authors from similar SLs in similar experimental conditions [13]. But in [13], the presence in the experimental spectra of modes “forbidden” in the deformation potential mechanism is not discussed. Usually, the Fröhlich mechanism has bright effects in Raman spectra in resonant conditions [2]. According to the calculated and experimental data [31], the minimal energies of optical transitions for SLs 1–3 (see Table 1) are 1.8, 1.91, and 2.02 eV. It is far

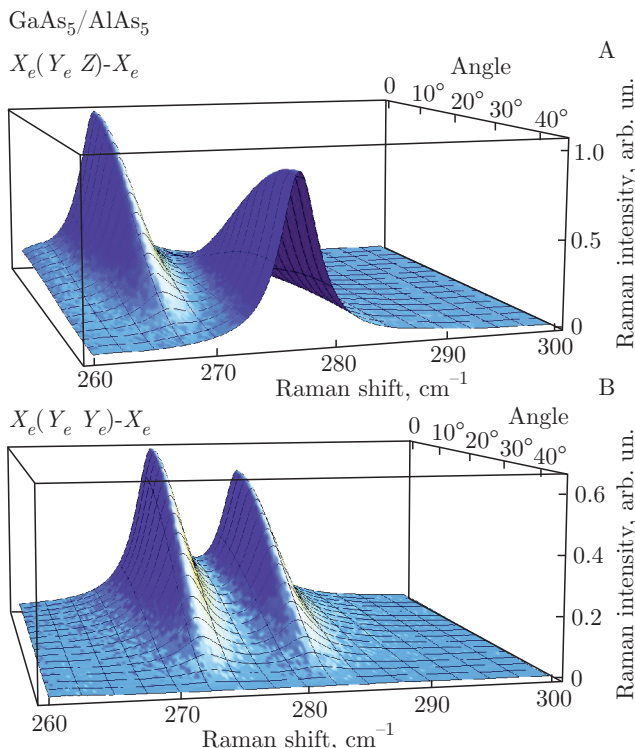


Fig. 4. Raman spectra of the $\text{GaAs}_5/\text{AlAs}_5$ superlattice calculated as functions of the angle measured from the axes $X'(110)$ and $X(100)$. A: “perpendicular” polarization geometry; B: “parallel” polarization geometry

from the energy of exiting photons in our case of an Ar^+ laser (2.41 eV). For such short-period SLs, the energies of direct optical transitions are higher than the energies of indirect ones [29]. High-energy direct optical transitions can play a role in Raman scattering, especially for the SLs with the shortest period. We can see the growth of the Raman signal in the $X(YY)-X$ geometry forbidden for the deformation potential mechanism with reducing the SL period (see Figs. 1–3). We can therefore suppose that at least for the shortest-period SL, the Raman scattering conditions are near-resonant, and hence the Fröhlich mechanism can take place in scattering.

It was also interesting to see how the selection rules depend on the direction of the wave vector. We have no experimental conditions to make the special cleavages oriented at any angles. But we can calculate the spectra for any direction of the wave vector. The results for $\text{GaAs}_5/\text{AlAs}_5$ SL are presented in Fig. 4. For the “perpendicular” polarization geometry (Fig. 4a), the zero angle corresponds to the $X'(ZY')-X'$ scattering geometry. Experimental spectra for this geometry were studied in [17]. In this case, the axes X' and Y' cor-

respond to crystallographic directions (110) and $(1\bar{1}0)$. For the angle equal to 45° , the scattering geometry is $X(ZY)-X$. As we can see from Fig. 4, there is no angular dependence of the phonon frequencies, but there is an angular dependence for selection rules. We see that the ratio between intensities of Raman peaks for different modes depends on the angle. For the “parallel” polarization geometry (Fig. 4b), the zero angle corresponds to the $X'(YY')-X'$ scattering geometry. Experimental spectra for this geometry were also studied in [17]. In this case, for the angle equal to 45° , the scattering geometry is the “forbidden” $X(YY)-X$. We see that the intensities of Raman peaks decrease with increasing the angle from zero to 45 degrees.

4. CONCLUSION

We have found significant differences between experimental Raman spectra of short-period GaAs/AlAs SLs with the wave vectors of the incident and scattered light lying in the plane of SLs and the spectra calculated taking the deformation potential and the electro-optical mechanisms of electron–phonon interactions into account. From comparing the experimental and calculated spectra, we can conclude that the Fröhlich mechanism can take place in Raman scattering for this experimental conditions of scattering.

The authors thank A. I. Toropov for having grown the superlattices.

REFERENCES

1. A. P. Silin, Sov. Phys. Usp. **28**, 972 (1985).
2. *Light Scattering in Solids V. Superlattices and Other Microstructures*, ed. by M. Cardona and G. Güntherodt, Springer-Verlag, Berlin (1989).
3. S. M. Rytov, Sov. Phys. JETP **2**, 466 (1955).
4. A. S. Barker, Jr., J. L. Merz, and A. C. Gossard, Phys. Rev. B **17**, 3181 (1978).
5. R. Merlin, C. Colvard, M. V. Klein, H. Morkoc, A. Y. Cho, and A. C. Gossard, Appl. Phys. Lett. **36**, 43 (1980).
6. B. Jusserand, D. Paquet, J. Kervarec, and A. Regeney, J. Phys. **45**, C5 (1984).
7. A. K. Sood, J. Menendez, M. Cardona, and K. Ploog, Phys. Rev. Lett. **54**, 2115 (1985).
8. M. Cardona, Superlatt. Microstruct. **5**, 27 (1989).

9. V. A. Volodin, M. D. Efremov, V. V. Preobrazhenskii, B. R. Semyagin, and V. V. Bolotov, Superlatt. Microstruct. **26**, 11 (1999).
10. A. Huber, T. Egeler, W. Ettmüller, H. Rothfritz, G. Trankle, and G. Abstreiter, Superlatt. Microstruct. **9**, 309 (1991).
11. R. Hessmer, A. Huber, T. Egeler, M. Haines, G. Trankle, G. Weimann, and G. Abstreiter, Phys. Rev. B **46**, 4071 (1992).
12. G. Scamarcio, M. Haines, G. Abstreiter, E. Molinari, S. Baroni, A. Fischer, and K. Ploog, Phys. Rev. B **47**, 1483 (1993).
13. A. Fainstein, P. Etchegoin, M. P. Chamberlain, M. Cardona, K. Totemeyer, and K. Eberl, Phys. Rev. B **51**, 14448 (1995).
14. M. Zunke, R. Schorer, G. Abstreiter, W. Klein, G. Weimann, and M. P. Chamberlain, Sol. St. Comm. **93**, 847 (1995).
15. V. A. Volodin, M. P. Sinyukov, V. A. Sachkov, M. Stoffel, H. Rinnert, and M. Vergnat, Europhys. Lett. **105**, 16003 (2014).
16. V. A. Volodin and M. P. Sinyukov, Pis'ma v Zh. Eksp. Teor. Fiz. **99**, 463 (2014).
17. V. A. Volodin, V. A. Sachkov, and M. P. Sinyukov, Zh. Eksp. Teor. Fiz. **147**, 906 (2015).
18. V. A. Volodin, V. A. Sachkov, and I. S. Golovin, Phys. Exp. **4**, 11 (2014).
19. Shang-Fen Ren, Hanyou Chu, and Yia-Chung Chang, Phys. Rev. B **37**, 8899 (1988).
20. Shang-Fen Ren and G. Qin, Sol. St. Comm. **121**, 171 (2002).
21. M. P. Chamberlain, M. Cardona, and B. K. Ridley, Phys. Rev. B **48**, 14356 (1993).
22. L. Miglio and L. Colombo, Superlatt. Microstruct. **7**, 139 (1990).
23. M. V. Vol'kenshtein, DAN SSSR **XXXII**, 185 (1941).
24. P. Castrillo, L. Colombo, and G. Armelles, Phys. Rev. B **49**, 10362 (1994).
25. *Study of the Lattice Dynamics of Low-dimensional Structures on the Basis of GaAs/AlAs Structures Using Numerical Simulations*, V. A. Sachkov, PhD Thesis, Omsk (2011).
26. L. N. Ovander and N. S. Tyu, Phys. Stat. Sol. (b) **91**, 763 (1979).
27. H. Fröhlich, Adv. Phys. **3**, 325 (1954).
28. W. Kauschke, A. K. Sood, M. Cardona, and K. Ploog, Phys. Rev. B **36**, 1612 (1987).
29. A. W. E. Minnaert, A. Yu. Silov, W. van der Vleuten, J. E. M. Haverkoff, and J. H. Wolter, Phys. Rev. B **63**, 075303 (2001).
30. A. Chernikov, V. Bornwasser, M. Koch, S. Chatterjee, C. N. Böttge, T. Feldmann, M. Kira, S. W. Koch, T. Wassner, S. Lautenschläger, B. K. Meyer, and M. Eickhoff, Phys. Rev. B **85**, 035201 (2012).
31. H. Fujimoto, C. Hamaguchi, T. Nakazava, K. Tamaguchi, K. Imanichi, H. Kato, and Y. Watanabe, Phys. Rev. B **41**, 7593 (1990).